ChemComm

COMMUNICATION

View Article Online
View Journal | View Issue

Cite this: *Chem. Commun.*, 2025, **61**, 18112

Received 19th August 2025,
Accepted 14th October 2025

DOI: 10.1039/d5cc04792g

rsc.li/chemcomm

A snapshot of flavin-conjugated Pt anticancer agents: Pt(IV)-to-Pt(II) reduction revealed by X-ray fluorescence imaging and XANES

Esteban Zingales, [abc] Juan Sanchez-Camacho, [ab] Jessica Walker, [d] Luca Salassa [abe] and Carlos Sanchez-Cano *[abe]

Synchrotron-based X-ray spectromicroscopy reveals enhanced cellular uptake and remarkably fast, efficient photoactivation of Pt(IV) prodrugs bearing flavin groups. These features correlate with superior anticancer activity compared to non-conjugated analogues, highlighting the potential of flavin-functionalised Pt(IV) complexes as candidates for photoactivated chemotherapy (PACT).

Pt(IV) prodrugs are a viable alternative to conventional Pt anticancer drugs due to their inertness and intracellular activation to cytotoxic Pt(II) species, which may help reduce systemic toxicity and resistance.[1] Photoactivated chemotherapy (PACT)[2] enables spatial and temporal control of this activation using light. Rapid and effective Pt(IV) reduction may be advantageous in minimizing the need for prolonged light irradiation and avoiding related side effects.[3] While several photoactivatable Pt(IV) complexes show promising *in vitro* anticancer activity,[4] their intracellular activation remains poorly characterised and often inefficient. For instance, only ~20% of an azido Pt(IV) complex was reduced to Pt(II) after 1 hour of blue light exposure—posing challenges for clinical applicability.[5]

In recent years, we have shown that flavins can efficiently and selectively photocatalyse the activation of Pt(IV) anticancer prodrugs, converting them into clinically used agents such as cisplatin, carboplatin, and oxaliplatin.[6–8] These reactions proceed in the presence of various (bio)reductants, which facilitate the excited-state generation of the catalytically active flavin hydroquinone species (Fig. 1A).[8,9] This transformation represents a rare example of photocatalytic functionalization of metal-based coordination complexes.[10,11] Notably, this reactivity extends beyond free flavins and is preserved when they are integrated into protein scaffolds or synthetic systems, including flavoenzymes,[12–14] hydrogels,[15] and nanozymes.[16]

We also investigated the covalent attachment of a flavin moiety—specifically 2′,3′,4′,5′-tetraacetylriboflavin (TARF)—to Pt(IV) precursors of cisplatin and oxaliplatin. This strategy yielded novel conjugates (**1·TARF** and **2·TARF**, Fig. 1B) with enhanced redox reactivity toward biological reductants, even in the absence of light.[17] Notably, these TARF-linked Pt(IV) complexes underwent rapid activation by NADH in the dark within minutes. Under photoirradiation, they also converted to Pt(II) drugs in the presence of glutathione—an outcome not observed with free flavins under catalytic conditions. This elevated reactivity translated into significantly improved antiproliferative activity of **2·TARF** in cancer cells, showing nearly a 100-fold enhancement when preincubated with non-toxic levels of ascorbate, compared to the effect of co-administered, unlinked

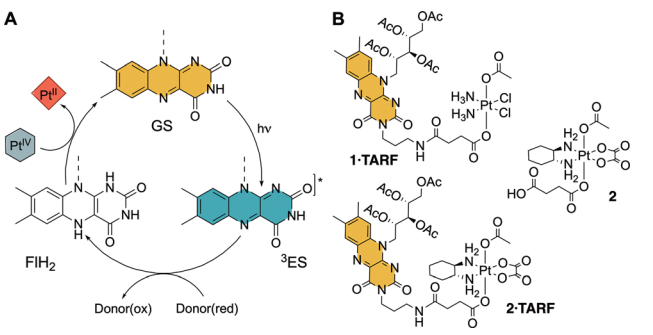

Fig. 1 (A) Mechanism for flavin-catalysed activation of Pt(IV) prodrugs (GS = ground state; ^{3}ES = triplet excited state; FlH$_2$ = flavin hydroquinone. (B) Structures of Pt(IV)-TARF complexes reported earlier (**1·TARF** and **2·TARF**)[17] and Pt(IV) complexes used in this study (**2·TARF** and **2**).

[a] *Donostia International Physics Center, Paseo Manuel de Lardizabal 4, Donostia-San Sebastian 20018, Spain. E-mail: carlos.sanchez@dipc.org*
[b] *Polimero eta Material Aurreratuak, Fisika, Kimika eta Teknologia, Kimika Fakultatea, Euskal Herriko Unibertsitatea UPV/EHU, 20018 Donostia-San Sebastian, Spain*
[c] *Center for Cooperative Research in Biomaterials (CIC biomaGUNE) Basque Research and Technology Alliance (BRTA), Paseo de Miramón 194, Donostia-San Sebastián 20014, Spain*
[d] *Diamond Light Source, Harwell Science and Innovation Campus, Didcot OX11 0DE, UK*
[e] *Ikerbasque, Basque Foundation for Science, Plaza de Euskadi 5, Bilbao 48009, Spain*

components. Concurrent work by Krasnovskaya *et al.*[18] demonstrated that a structurally related TARF–Pt(IV) cisplatin prodrug exhibited *in vitro* anticancer activity upon blue light irradiation, operating through a combination of photodynamic therapy (PDT) and PACT depending on the light dose. Notably, this study also provided electrochemical evidence for the reduction of the flavin–Pt conjugate within cell spheroids, leading to cisplatin release. Yet, the efficiency of Pt(IV) reduction could not be quantified.

Synchrotron-based X-ray microscopy and spectroscopy techniques are ideal methods to analyse metals in biological environments.[19] X-rays enable direct probing of metals to investigate their electronic, chemical, and structural properties, as well as to perform label-free elemental imaging. Techniques like X-ray Fluorescence Imaging (XFI)[20] and X-ray Absorption Spectroscopy (XAS)[21] can provide information relevant for multiple fields related to biology. XFI probes inner-shell electrons to produce element-specific emissions,[20] and enables simultaneous 2D or 3D mapping of multiple elements with high sensitivity and resolutions from several μm^2 to below $20 \times 20\ nm^2$. As such, XFI has been used to determine the distribution of metallodrugs inside bacteria or mammalian cells with subcellular resolution.[22–25] Complementarily, X-ray Absorption Spectroscopy (XAS) characterises the chemical state, electronic structure, and local atomic environment of elements by measuring their X-ray absorption at varying energies. XANES probes electron binding energies, while EXAFS analyses elastic scattering of photoelectrons from neighboring atoms. Correlative XFI–XAS analyses at nanoprobe beamlines enable spatially resolved mapping of metallodrug chemical transformations within cells, and have been used to study the activation of Pt- and other metal-based prodrugs.[5,26]

In this context, we employed synchrotron-based spectromicroscopy to investigate the *in cellulo* localization and oxidation state of complexes **2·TARF** and **2** (Fig. 1B), aiming to gain deeper insight into the intracellular activation efficiency of Pt-TARF derivatives and to advance our understanding of metal–flavin interactions and their biological effects.

Probing the photoactivation efficiency of **2·TARF** and related prodrugs in cellular environments with X-rays is challenging, as it is difficult to distinguish Pt(II) species generated by photo-induced Pt(IV) reduction from those produced by endogenous cellular reductants in the dark. Our previous studies demonstrated that **2** is non-toxic across multiple cell lines.[17] However, direct conjugation to TARF led to a moderate enhancement of the dark antiproliferative activity of the Pt(IV) prodrug **2**, likely due to improved cellular uptake driven by TARF's lipophilicity and increased redox responsiveness imparted by the flavin moiety. Collectively, these findings suggest that TARF coupling promotes more rapid and efficient intracellular reduction, thereby accelerating the release of the active Pt(II) species.

To minimise unwanted dark Pt(IV) → Pt(II) reduction, we optimised experimental conditions for photoactivation studies. Different incubation times were tested to achieve adequate intracellular Pt levels for X-ray detection while avoiding dark toxicity. Light irradiation effects were also considered, as Pt(II) quantification must be performed immediately post-irradiation to prevent interference from time-dependent cellular changes. Thus, we

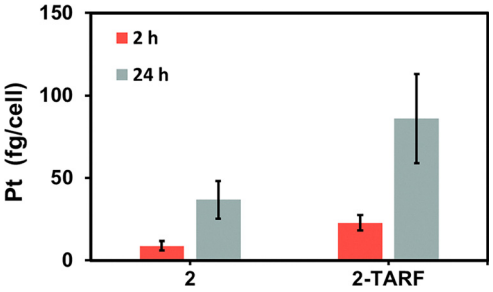

Fig. 2 Cellular accumulation of Pt (fg/cell) in MCF7 human breast epithelial adenocarcinoma cells after treatment with **2** or **2·TARF** (50 μM) in the dark, as measured by ICP-MS.

investigated the photoactivation of **2·TARF** in MCF-7 human breast adenocarcinoma cells, selected for their prior use in related cellular studies.[17] Cells were exposed to the prodrug for short incubation periods and irradiated with low light doses. Immediately following irradiation, they were fixed and stored in the dark to prevent unintended photoreduction of residual prodrug prior to intracellular platinum analysis by X-ray spectromicroscopy (XFI and XANES). This approach ensured that the activation of **2·TARF** was primarily driven by the irradiation process, minimizing confounding effects from cell death, damage-related reduction, or spontaneous reduction under physiological or storage conditions (see SI for experimental details).

Cell accumulation of the prodrugs was initially assessed in bulk samples after treatment of MCF7 cells with 50 μM solutions of either **2** or **2·TARF** for 2 or 24 h in the dark (Fig. 2 and Table S1, SI). ICP-MS analysis of the cell pellets obtained showed time-dependent internalisation of both complexes, with around 4-fold more platinum found inside cells after incubations of 24 h than in cells treated for 2 h. Additionally, the presence of the flavin moiety increased the internalisation of the complexes: cells treated with **2·TARF** exhibited a 2.5-fold increase (approx.) in platinum content relative to those treated with **2**, regardless of incubation duration (Fig. 2 and Table S1, SI). Based on these findings, a 2-hour incubation was selected for subsequent experiments, as it offered an optimal balance between sufficient intracellular platinum accumulation—within the detection limits of the X-ray spectromicroscopy[20,27] and the absence of dark cytotoxicity.[17,18] This minimised the likelihood of unwanted Pt(IV) reduction under non-irradiated conditions.

Next, we conducted synchrotron-based spectromicroscopy experiments to confirm the intracellular accumulation of **2** and **2·TARF**, and to assess the photoactivation efficiency of **2·TARF** in MCF7 human breast adenocarcinoma cells. Cells were cultured on carbon-framed Si_3N_4 membrane windows (see SI for full details) and incubated in the dark for 2 h with 50 μM of the respective complexes. Following incubation, the drug-containing media were removed, and the cells were irradiated for three minutes with low-intensity blue light (460 nm, 0.1 mW cm^{-2}; total dose: 18 mJ cm^{-2}). This light dose is significantly lower than those previously reported for the photoactivation of Pt(IV) prodrugs, yet sufficient to achieve complete photoreduction of **2·TARF** in solution,[17] and remains well below the phototoxic threshold for

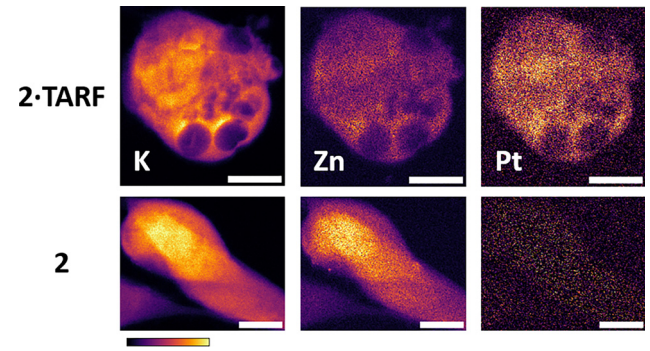

Fig. 3 XFI elemental maps comparing the intracellular distribution density of K K_α (0–100 ng mm^{-2}), Zn K_α (0–0.9 ng mm^{-2}), Pt L_α (0–0.25 ng mm^{-2}) within cryo-fixed and freeze-dried MCF7 cells irradiated with blue light (460 nm, 0.1 mW cm^{-2}, 18 mJ cm^{-2}) after treatment with 50 μM **2·TARF** or **2** for 2 h. Maps were collected with 60 or 75 nm step size and 200 ms dwell time, processed using PyMca,[29] and images were generated using ImageJ.[30] Scale bars are 5 μm.

cultured cells. Furthermore, the irradiation conditions were selected to minimise singlet oxygen generation by the flavin moiety,[6] thus avoiding potential non-specific photodamage or unintended prodrug activation pathways. Post-treatment, samples were vitrified in liquid propane and dehydrated using freeze-drying. Spectromicroscopy was performed at room temperature on the I14 Hard X-ray Nanoprobe beamline (Diamond Light Source, UK) using a monochromatic X-ray beam (full details in the SI).[28]

XFI enabled visualization of element distributions in cryo-fixed, dehydrated MCF7 cells (Fig. 3 and Fig. S1–S8, SI), including biologically relevant elements like K and Zn, and the exogenous element Pt. K and Zn K-emission maps outlined overall cell morphology and nuclear localization, while Pt L-emission maps revealed the intracellular distribution of **2** and **2·TARF** (Fig. S9, SI). Correlative phase contrast imaging indicated structural changes, including drug-related damage, with **2·TARF**-treated cells displaying less defined nuclei than those treated with **2**.

Pt L-emission was detected in all treated samples (Fig. S1, SI), and comparison with an elemental standard (SI) enabled semi-quantitative estimation of Pt accumulation per cell. Although XFI-based Pt levels were lower than those from ICP-MS (between 4 and 6-fold), they were in the same range, and such discrepancies are expected given XFI's semi-quantitative nature.[20] Notably, XFI still showed ~3-fold higher Pt levels in **2·TARF**-treated cells compared to those treated with **2**, in agreement with ICP-MS results (Table S3, SI).

Pt XFI revealed that, once internalised, **2** was distributed homogeneously throughout the cells, consistent with previous observations for similar photoactivatable Pt(IV) prodrugs.[5] The incorporation of the flavin moiety in **2·TARF** enhanced cellular accumulation but did not alter its intracellular distribution, as Pt remained evenly distributed. Notably, cells treated with **2·TARF** exhibited increased markers of cellular stress (Fig. 3 and Fig. S3–S8, SI), even following short irradiation times. This was further supported by morphological changes, as **2·TARF**-treated cells appeared smaller and more rounded compared to those treated with **2** (Table S4, SI). These findings suggest that the enhanced anticancer activity of flavoplatin prodrugs relative to their non-flavinated counterparts under light irradiation can manifest rapidly, even after brief exposure. Consistent with flavin redox (photo)chemistry, a plausible explanation is the generation of high levels of reactive radical species during the photoactivation of **2·TARF**, although this hypothesis requires further investigation.

To assess the intracellular photoactivation efficiency of prodrugs **2** and **2·TARF** XANES mapping was performed on regions with the highest Pt accumulation, as identified by prior XFI maps (Fig. 4A). For each region studied, 150 consecutive XFI maps (200 × 200 nm^2 step size) were collected using X-rays across the Pt–L_3 edge (starting energy 11 465 eV, 300 eV range). These were used to generate pixel-resolved XANES spectra by integrating the Pt–L emission intensity at each excitation energy. PCA and cluster analysis, performed using the MANTIS software,[31] identified regions of similar spectral features—reflecting Pt speciation (Fig. 4A and B). Reference XANES spectra were also collected from Pt standards with defined Pt(IV)/Pt(II) ratios (Fig. 4C, and Fig. S10, S11, SI).

Due to low Pt levels, cells exposed to **2** did not yield usable XANES spectra. In contrast, for cells exposed to **2·TARF** and irradiated, the Pt(II)/Pt(IV) ratio was determined using multiple methods (SI), including: (i) linear combination fitting (LCF) with Pt standards, and (ii) linear regression calibration using all previously described standards, based on the a/b ratio between the edge maximum (a) and the post-edge minimum following the white line (b).[32] Both approaches produced consistent results (Fig. 4D and Fig. S11, S12, SI).

Our analysis indicated that Pt(IV) activation was homogeneous throughout **2·TARF**-treated cells, with over 70% of intracellular Pt

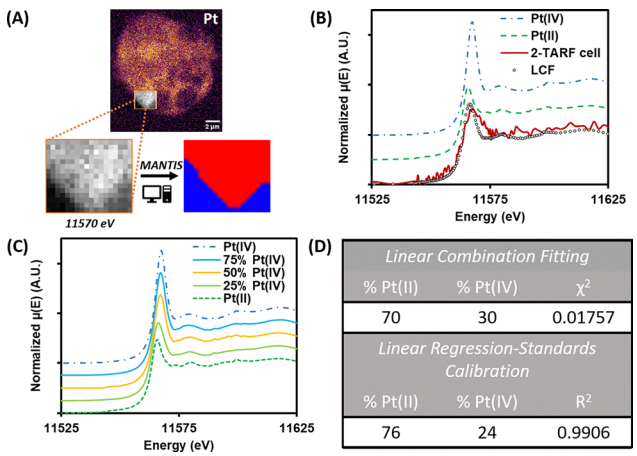

Fig. 4 (A) Pt XFI map showing area studied by XANES mapping on a MCF7 cell treated with **2·TARF** and irradiated with blue light. Zoom shows XFI map acquired at a single energy during XANES mapping; in red, regions used for Pt speciation analysis as segmented by MANTIS.[31] (B) Normalised XANES spectra of Pt(IV) and Pt(II) standards, extracted from cell in (A), and linear combination fitting (LCF) of sample using both standards. (C) Normalised XANES spectra of standards with different Pt(IV) and Pt(II) content (%Pt(II) in each standard: 100–%Pt(IV)). (D) %Pt(II) and %Pt(IV) in XANES extracted from cell in (A), as determined by LCF or linear regression–standard calibration methods.[32]

reduced to Pt(II) under the low blue light dose applied (18 mJ cm^{-2}). Remarkably, this extent of photoactivation and release of active Pt species is unprecedented when compared to similar non-flavinated Pt(IV) prodrugs bearing hydroxide axial ligands, which show only ~20% intracellular reduction even under much higher irradiation doses (17 J cm^{-2}) using the same methodology.[5] Given our experimental design—aimed at minimizing prodrug reduction in the dark within the cellular environment—and the low anticancer activity of **2** under both dark conditions and external reducing stimuli (*e.g.*, ascorbate co-treatment or blue light irradiation),[17,18] these findings support that the efficient photo-reduction of **2**·**TARF** and the associated release of active oxaliplatin species observed in solution after brief irradiation also occurs within cellular environments.[17]

In conclusion, conjugation of a **TARF** fragment to a Pt(IV) anticancer prodrug enhances cellular accumulation without affecting intracellular distribution and enables remarkably high levels of photo-induced Pt(IV) → Pt(II) reduction under minimal light exposure. This pronounced photoactivation was directly demonstrated in cells under carefully controlled conditions. Such a property in flavin-conjugated Pt(IV) hybrids holds strong promise for PACT applications, particularly under hypoxic conditions where conventional flavin-based photosensitization effects may be limited.

The authors thank the Spanish State Research Agency MICIU/AEI/10.13039/501100011033 (PID2020-118176RJ-I100, PID2022-139267OB-I00 and PRE2020-093560) and Basque Government-Eusko Jaurlaritza (Elkartek KK-2023/00003; IT1584-22) for funding. DIPC was supported by the Severo Ochoa Grant CEX2024-001494-S funded by MICIU/AEI/10.13039/501100011033. SGIKER (UPV/EHU/ERDF, EU) is acknowledged for technical and human support. This work was carried out with the support of Diamond Light Source, beamline I14 (proposal MG33156).

Conflicts of interest

There are no conflicts of interest to declare.

Data availability

Data for this article, including raw and processed XFI and XANES maps, and XANES standards are available at Zenodo.org at **https://doi.org/10.5281/zenodo.16892322**.

The rest of the data is contained within the article or the supplementary information (SI). Supplementary information is available. See DOI: **https://doi.org/10.1039/d5cc04792g**.

Notes and references

1 T. C. Johnstone, K. Suntharalingam and S. J. Lippard, *Chem. Rev.*, 2016, **116**, 3436.
2 N. J. Farrer, L. Salassa and P. J. Sadler, *Dalton Trans.*, 2009, 10690.
3 K. Moloudi, H. Abrahamse and B. P. George, *Biomed. J.*, 2025, **4**, 100889.
4 J. Gurruchaga-Pereda, A. Martinez, A. Terenzi and L. Salassa, *Inorg. Chim. Acta*, 2019, **495**, 118981.
5 E. M. Bolitho, C. Sanchez-Cano, H. Shi, P. D. Quinn, M. Harkiolaki, C. Imberti and P. J. Sadler, *J. Am. Chem. Soc.*, 2021, **143**, 20224.
6 S. Alonso-de Castro, S. A. Terenzi, S. Hager, B. Englinger, A. Faraone, J. C. Martínez, M. Galanski, B. K. Keppler, W. Berger and L. Salassa, *Sci. Rep.*, 2018, **8**, 17198.
7 S. Alonso-de Castro, E. Ruggiero, A. Ruiz-de-Angulo, E. Rezabal, J. C. Mareque-Rivas, X. Lopez, F. López-Gallego and L. Salassa, *Chem. Sci.*, 2017, **8**, 4619.
8 J. Gurruchaga-Pereda, V. Martínez-Martínez, E. Rezabal, X. Lopez, C. Garino, F. Mancin, A. L. Cortajarena and L. Salassa, *ACS Catal.*, 2020, **10**, 187.
9 S. Scoditti, E. Dabbish, G. E. Pieslinger, E. Rezabal, X. Lopez, E. Sicilia and L. Salassa, *Phys. Chem. Chem. Phys.*, 2022, **24**, 5323.
10 F. López-Gallego and L. Salassa, *Chem Catal.*, 2023, **3**, 100459.
11 G. Salassa and L. Salassa, *ACS Omega*, 2021, **6**, 7240.
12 S. Alonso-de Castro, A. L. Cortajarena, F. López-Gallego and L. Salassa, *Angew. Chem., Int. Ed.*, 2018, **57**, 3143.
13 J. Gurruchaga-Pereda, V. Martínez-Martínez, E. Formoso, O. Azpitarte, E. Rezabal, X. Lopez, A. L. Cortajarena and L. Salassa, *J. Phys. Chem. Lett.*, 2021, **12**, 4504.
14 L. F. Mazzei, J. Gurruchaga-Pereda, A. Martínez, J. C. Martínez, L. Salassa and A. L. Cortajarena, *Chem. Commun.*, 2023, **59**, 4754.
15 S. Velasco-Lozano, S. Alonso-de Castro, C. Sanchez-Cano, A. I. Benítez-Mateos, F. López-Gallego and L. Salassa, *Chem. Sci.*, 2022, **13**, 59.
16 L. F. Mazzei, A. Martínez, L. Trevisan, D. Rosa-Gastaldo, A. L. Cortajarena, F. Mancin and L. Salassa, *Chem. Commun.*, 2020, **56**, 10461.
17 J. Sánchez-Camacho, S. Infante-Tadeo, A. C. Carrasco, S. Scoditti, A. Martínez, F. Barroso-Bujans, E. Sicilia, A. Pizarro and L. Salassa, *Inorg. Chem.*, 2023, **62**, 5644.
18 O. O. Krasnovskaya, R. A. Akasov, D. V. Spector, K. G. Pavlov, A. A. Bubley, V. A. Kuzmin, A. A. Kostyukov, E. V. Khaydukov, E. V. Lopatukhina, A. S. Semkina, A. S. K. Y. Vlasova, S. A. Sypalov, A. S. Erofeev, P. V. Gorelkin, A. N. Vaneev, V. N. Nikitina, D. A. Skvortsov, D. A. Ipatova, D. M. Mazur, N. V. Zyk, D. A. Sakharov, A. G. Majouga and E. K. Beloglazkina, *ACS Appl. Mater. Interfaces*, 2023, **15**, 12882.
19 D. J. Hare, E. J. New, M. D. de Jongee and G. McColl, *Chem. Soc. Rev.*, 2015, **44**, 5941.
20 M. J. Pushie, N. J. Slvain, H. Hou, M. J. Hackett, M. E. Kelly and S. M. Webb, *Metallomics*, 2022, **14**, mfac032.
21 A. G. Buzanich, *X-Ray Spectrom.*, 2022, **51**, 294.
22 F. Fus, Y. Yang, H. Z. S. Lee, S. Top, M. Carriere, A. Bouron, A. Pacureanu, J. C. da Silva, M. Salmain, A. Vessières, P. Cloetens, G. Jaouen and S. Bohic, *Angew. Chem., Int. Ed.*, 2019, **58**, 3461.
23 J. J. Conesa, A. C. Carrasco, V. Rodríguez-Fanjul, Y. Yang, J. L. Carrascosa, P. Cloetens, E. Pereiro and A. M. Pizarro, *Angew. Chem., Int. Ed.*, 2020, **59**, 1270.
24 E. M. Bolitho, J. P. C. Coverdale, H. E. Bridgewater, G. J. Clarkson, P. D. Quinn, C. Sanchez-Cano and P. J. Sadler, *Angew. Chem., Int. Ed.*, 2021, **60**, 6462.
25 M. Draveny, M. Draveny, H. Chauvet, V. Rouam, F. Jamme and M. Masi, *ACS Nano*, 2025, **19**, 979.
26 C. Sanchez-Cano, D. Gianolio, I. Romero-Canelon, R. Tucoulou and P. J. Sadler, *Chem. Commun.*, 2019, **55**, 7065.
27 J. Decelle, G. Veronesi, B. Gallet, H. Stryhanyuk, P. Benettoni, M. Schmidt, R. Tucoulou, M. Passarelli, S. Bohic, P. Clode and N. Musat, *Trends Cell Biol.*, 2020, **30**, 173.
28 P. D. Quinn, L. Alianelli, M. Gomez-Gonzalez, D. Mahoney, F. Cacho-Nerin, A. Peach and J. E. Parker, *J. Synchrotron Radiat.*, 2021, **28**, 1006.
29 V. A. Solé, E. Papillon, M. Cotte, P. Walter and J. Susini, *Spectrochim. Acta, Part B*, 2007, **62**, 63.
30 J. Schindelin, I. Arganda-Carreras, E. Frise, V. Kayning, M. Longair, T. Pietzsch, S. Preibisc, C. Rueden, S. Saalfeld, B. Schmid, J. Y. Tinevez, D. J. White, V. Hartenstein, K. Eliceiri and P. Tomancak, *Nat. Methods*, 2012, **9**, 676.
31 M. Lerotic, R. Mak, S. Wirick, F. Meirer and C. Jacobsen, *J. Synchrotron Radiat.*, 2014, **21**, 1206.
32 M. D. Hall, G. J. Foran, M. Zhang, P. J. Beale and T. W. Hambley, *J. Am. Chem. Soc.*, 2003, **125**, 7524.